Molecular Therapy
Nucleic Acids
Original Article

G-Quadruplex-Forming DNA Aptamers Inhibit the DNA-Binding Function of HupB and *Mycobacterium tuberculosis* Entry into Host Cells

Priya Kalra,[1] Subodh Kumar Mishra,[2] Surinder Kaur,[1] Amit Kumar,[2] Hanumanthappa Krishna Prasad,[1] Tarun Kumar Sharma,[3] and Jaya Sivaswami Tyagi[1,3]

[1]Department of Biotechnology, All India Institute of Medical Sciences, New Delhi, Delhi 110029, India; [2]Discipline of Biosciences and Biomedical Engineering, Indian Institute of Technology Indore, Simrol, Madhya Pradesh 453552, India; [3]Centre for Biodesign and Diagnostics, Translational Health Science and Technology Institute, Faridabad, Haryana 121001, India

The entry and survival of *Mycobacterium tuberculosis* (*Mtb*) within host cells is orchestrated partly by an essential histone-like protein HupB (Rv2986c). Despite being an essential drug target, the lack of structural information has impeded the development of inhibitors targeting the indispensable and multifunctional C-terminal domain (CTD) of HupB. To bypass the requirement for structural information in the classical drug discovery route, we generated a panel of DNA aptamers against HupB protein through systemic evolution of ligands by exponential (SELEX) enrichment. Two G-quadruplex-forming high-affinity aptamers (HupB-4T and HupB-13T) were identified, each of which bound two distinct sites on full-length HupB, with an estimated K_D of ~1.72 μM and ~0.17 μM, respectively, for the high-affinity sites. While HupB-4T robustly inhibited DNA-binding activity of HupB *in vitro*, both the aptamers recognized surface-located HupB and significantly blocked *Mtb* entry into THP-1 monocytic cells ($p < 0.0001$). In summary, DNA aptamers generated in this study block DNA-binding activity of HupB, inhibit virulent *Mtb* infection in host cells, and demonstrate aptamers to be inhibitors of HupB functions. This study also illustrates the utility of SELEX in developing inhibitors against essential targets for whom structural information is not available.

INTRODUCTION

Tuberculosis caused by *Mycobacterium tuberculosis* (*Mtb*) continues to be a major public health challenge. Owing to high mortality rates and emergence of drug-resistant *Mtb*, it has become necessary to search for novel drug targets and therapeutic reagents.[1] Bacterial constituents that are crucial for the survival of this pathogen are generally considered to be attractive drug targets. Therefore, it is logical to propose that interception or inhibition of these essential targets would effectively inhibit or kill both the drug-resistant and susceptible forms of *Mtb* alike. The nucleoid-associated histone-like protein HupB (Rv2986c; also known as HlpMt, MtbHU, MtHU, MDP1, LBP, Irep-28) is an essential protein in pathogenic mycobacteria and is consequently acknowledged as a promising drug target.[2,3] The indispensable nature of HupB is attributed to its ability to maintain the nucleoid architecture and protect mycobacterial DNA particularly under stressful environments, such as in presence of reactive oxygen species (Fenton's reaction) as well as DNase I-mediated digestion.[4–6] Besides mediating bacillary entry (dissemination and/or infectivity) into host cells by virtue of its function as a surface adhesin,[7] HupB also critically regulates iron homeostasis, imperative for *Mtb* survival in nutrient-deprived conditions of intracellular infection.[8] Consistent with its described functions, an *Mtb ΔhupB* mutant exhibited low infectivity and was unable to survive within host macrophages.[8]

A major challenge in designing structure-based inhibitors of *Mtb* HupB protein is the intrinsically disordered structure of its C-terminal domain (CTD), which precludes obtaining structural data. While HupB binds to DNA via the conserved N-terminal domain (NTD), its activity is modulated by its indispensable C terminus.[4,5] This activity of HupB indirectly modulates mycobacterial susceptibility to the TB drug Isoniazid; HupB inhibits the transcription of *katG* gene, which encodes catalase-peroxidase, the Isoniazid-activating enzyme.[4] The expression of HupB is elevated under intra-phagosomal milieu-like stress conditions such as nutrient starvation, hypoxia, and iron starvation, and low KatG levels is believed to contribute to bacterial tolerance to Isoniazid in these conditions.[4,9,10] Diarylethene derivatives that perturb the DNA-binding function of the HupB-NTD have been characterized recently.[11,12] However, inhibitors targeting full-length HupB are expected to be more potent in curtailing bacterial entry, mycobacterial growth, and dissemination, while simultaneously enhancing bacterial sensitivity to Isoniazid.[4,11,13] Because structural details of HupB available so far are insufficient to pursue

Received 9 June 2018; accepted 16 August 2018;
https://doi.org/10.1016/j.omtn.2018.08.011.

Correspondence: Jaya Sivaswami Tyagi, Department of Biotechnology, All India Institute of Medical Sciences, New Delhi, Delhi 110029, India.
E-mail: jayatyagi.aiims@gmail.com
Correspondence: Tarun Kumar Sharma, Centre for Biodesign and Bioengineering, Translational Health Science and Technology Institute, Faridabad, Haryana 121001, India.
E-mail: tarun@thsti.res.in

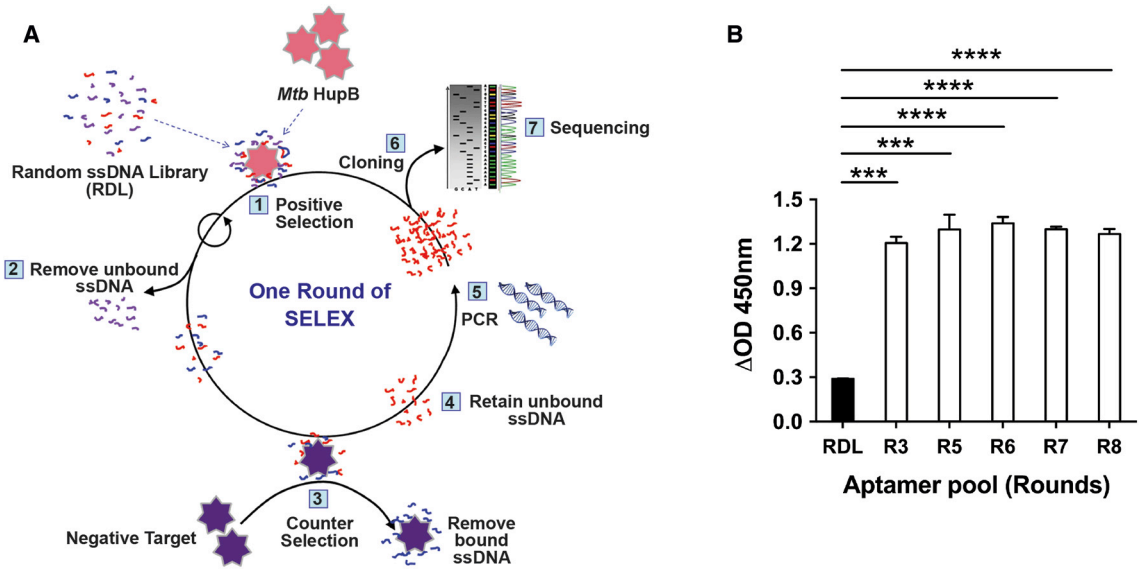

Figure 1. Systemic Evolution of Ligands by Exponential Enrichment

(A) Schema of subtractive SELEX consisting of steps including (1) positive selection, (2) partitioning, (3) counter-selection, and (4 and 5) elution of binders and amplification. After increasingly stringent rounds of SELEX, the highest affinity HupB-targeting aptamer pool was cloned (6) and colonies sequenced (7) to obtain potential aptamer candidates against HupB for further characterization. (B) Round-wise enrichment of HupB-binding oligonucleotide pools (rounds 3 and 5–8) by SELEX with respect to the starting random DNA library (RDL) assessed by ALISA (***$p \leq 0.005$, ****$p \leq 0.001$). Bars represent mean ± SD. See also Figure S1 and Table S1.

the classical drug discovery approach, we adopted the approach of designing and generating target-specific DNA aptamers to bypass this limitation. DNA aptamers of high affinity and specificity are considered as promising therapeutic reagents owing to their high stability, efficient binding, high selectivity, and no or minimal toxicity.[14,15] Previously, aptamers have shown their potential in antagonizing dissemination, penetration, and survival of dreaded pathogens within the host, such as Ebola virus, SARS, carbapenem-resistant Enterobacteriaceae (CRE), etc., thereby imparting successful and immediate passive immunity.[16]

Accordingly, in this study, we have developed a panel of high-affinity G-quadruplex-forming DNA aptamers against HupB through a subtractive systemic evolution of ligands by exponential (SELEX) strategy and extensively characterized them by various biochemical and biophysical techniques such as aptamer-linked immobilized sorbent assay (ALISA), isothermal titration calorimetry (ITC), circular dichroism (CD), native PAGE, etc. The generated aptamers targeted *Mtb* HupB protein with high affinity and selectivity and inhibited HupB-associated functions, including DNA binding and *Mtb* entry in THP-1 cells. To the best of our knowledge, this is the first report of an inhibitor targeting the disordered full-length HupB protein of virulent *Mtb*. This study exemplifies a strategy for developing potent aptamer-based inhibitors against *Mtb* targets for which no or incomplete structural information is available. These HupB-inhibitory aptamers are proposed to be anti-TB reagents with the potential to block essential functions of HupB in *Mtb*.

RESULTS

Generation of Aptamers Targeting the HupB Protein of *Mtb* by SELEX

A subtractive SELEX strategy was designed (Figure 1A) to obtain high-affinity single-stranded DNA (ssDNA) aptamers targeting *Mtb* HupB protein. SELEX was initiated using an equimolar mixture of three 80-nt-long random ssDNA libraries (RDLs; IDT USA) that were designed to have (1) 18-nt-long primer-binding sequences at the 5′ and 3′ ends, (2) a 3-nt-long sequence unique to each library (sequence tag) to facilitate post-SELEX identification of the starting library, and (3) a central unbiased or G-quadruplex-biased 41-nt random region (Table S1). After each round of SELEX, PCR amplification of HupB-specific ssDNA oligonucleotides was optimized to achieve maximum amplification without non-specific products (Figure S1A). A PCR master mix containing *Taq* DNA polymerase, having a high error rate (2.2×10^{-5} per nt per cycle) was utilized during amplification to promote diversity of the aptamer library.[17] The double-stranded (ds) PCR products obtained were converted to ss form, prior to successive SELEX rounds, as described in the Materials and Methods (Figure S1B). After eight rounds of SELEX, the enrichment of HupB-specific aptamers was assessed by ALISA. The ssDNA pools from archived round (R) 3, 5, 6, 7, and 8 populations were observed to bind to HupB protein ≥ 4 fold more efficiently than the starting RDL (RDL versus R3 or R5, $p \leq 0.005$; RDL versus R6, R7, or R8, $p \leq 0.001$; Figure 1B). The binding was saturated from R3 onward, and the aptamer pool from the last round (R8) was cloned and colonies were randomly picked and sequenced.

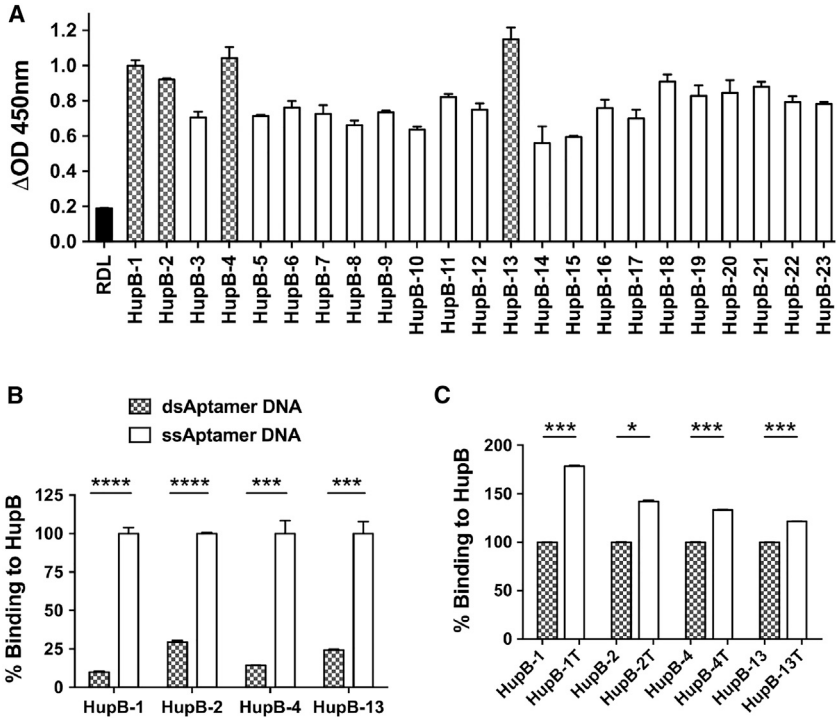

Figure 2. Selection of Aptamer Candidates and Post-SELEX Optimization

(A) ALISA was carried out with 7.6 nM 5′-biotinylated RDL and 23 ssDNA aptamer candidates. HupB-1, HupB-2, HupB-4, and HupB-13 aptamers exhibited highest binding (>5 fold over RDL) to HupB protein (checkered bars). See also Figure S2 and Table S2. (B) Binding of HupB-1, HupB-2, HupB-4, and HupB-13 aptamers (50 nM) in ssDNA and dsDNA forms to HupB protein assessed by ALISA. (C) Binding property of truncated (T) aptamers (~44 nt, 50 nM) to HupB relative to their full-length counterparts (~80 nt, 50 nM) was assessed by ALISA. (*$p < 0.05$, ***$p < 0.005$, ****$p < 0.001$). Bars represent mean ± SD.

In total, sequences of 23 unique clones were obtained and analyzed using online ClustalW (https://www.genome.jp/tools-bin/clustalw) and BioEdit (v7.2.5) software. These sequences are deposited at the Indian Patent office, under patent application no. 201711001246. Relative to the starting RDL that had an ~44-nt central region, mutations such as deletion was observed in HupB-9 (41 nt) and HupB-8 (43 nt) aptamers, while insertions were obtained in HupB-4, -6, -7, -22 (45 nt), and HupB-12 (48 nt) aptamers. Since the flanking primer-binding sites were common to all oligos, *in silico* analysis was restricted to the central nucleotide sequences (Figure S2A). Sequence analysis data revealed that out of 23 aptamers, nearly 70% (16 in number) of aptamers emerged from G-quadruplex-biased libraries, whereas 30% were derived from the unbiased library (TCG tag). Among these, of 16 aptamers from G-quadruplex-biased libraries, 11 originated from the 50% G-rich library (TAG tag), and the remaining 5 candidates were from 60% G+T rich library (TTG tag). Nucleotide composition analysis showed that irrespective of the starting RDL, (1) 11/23 oligos were T rich (≥30% T), (2) 13/23 oligos were G rich (≥30% G), and (3) nearly ~96% (22/23 oligos) had ≥60% G+T nucleotide content, suggesting a role for G+T content in mediating aptamer binding to HupB (Figure S2B). Phylogenetic tree analysis based on primary sequence homology revealed that the aptamers could broadly be categorized into three preponderant groups (Figure S2C). All 23 aptamers were screened using the Multiple Em for Motif Elicitation (MEME) online tool (http://meme-suite.org) to identify a conserved motif. The MEME output predicted 15 motifs ranging from 4 to 14 nt in length among the oligonucleotide sequences, based on statistical significance or low *E* value (Table S2). The most frequently present motif, Motif-1, which also displayed the lowest *E* value, was present at eight sites in eight oligonucleotides (HupB-2, -5, -6, -7, -9, -11, -14, and -18).

Identification of HupB-Targeting Aptamers

To identify aptamers having the highest binding efficiency, the HupB-binding potential of each of the 23-aptamer candidates was evaluated by ALISA. In brief, 5′-biotin-labeled ssDNA (~80 nt) was prepared for each of the 23 candidates by PCR amplification and converted to ss form as described in the Materials and Methods. All the aptamer candidates exhibited ≥3 fold higher binding to HupB than the initial random DNA library (RDL). Four aptamer candidates, namely, HupB-1, HupB-2, HupB-4, and HupB-13, displayed the highest binding to HupB (≥5 fold relative to RDL) and were selected for further study (checkered bars, Figure 2A).

Aptamers Selectively Bind HupB in the ss Form

HupB is a naturally occurring dsDNA-binding histone-like protein of *Mtb*. On the other hand, aptamers are highly structured ssDNA molecules that evince binding to their cognate target by acquiring complex 2D and 3D structures. Therefore, 5′-biotinylated HupB-1, HupB-2, HupB-4, and HupB-13 aptamers were assessed for their ability to bind HupB in their ss (~80 nt) or ds (~80 bp) forms. All four ssDNA aptamer candidates, HupB-1, HupB-2, HupB-4, and HupB-13, outperformed their respective dsDNA counterparts and exhibited superior binding to HupB (ds versus ss, HupB-1 and HupB-4, $p \leq 0.001$; HupB-2 and HupB-13, $p \leq 0.005$; Figure 2B). Notably, despite the natural ability of HupB to interact with dsDNA, the selected aptamers bound HupB with greater efficiency as ssDNA conformers compared to their respective ds counter-parts, emphasizing the importance of secondary structure configuration in binding.

Post-SELEX Optimization of Aptamers

Next, the flanking 18nt primer-binding sites common to all oligonucleotides were removed to generate truncated aptamers (~44 nt). An enhanced binding of all four truncated aptamers to HupB was observed by ALISA, relative to their respective ~80-nt full-length

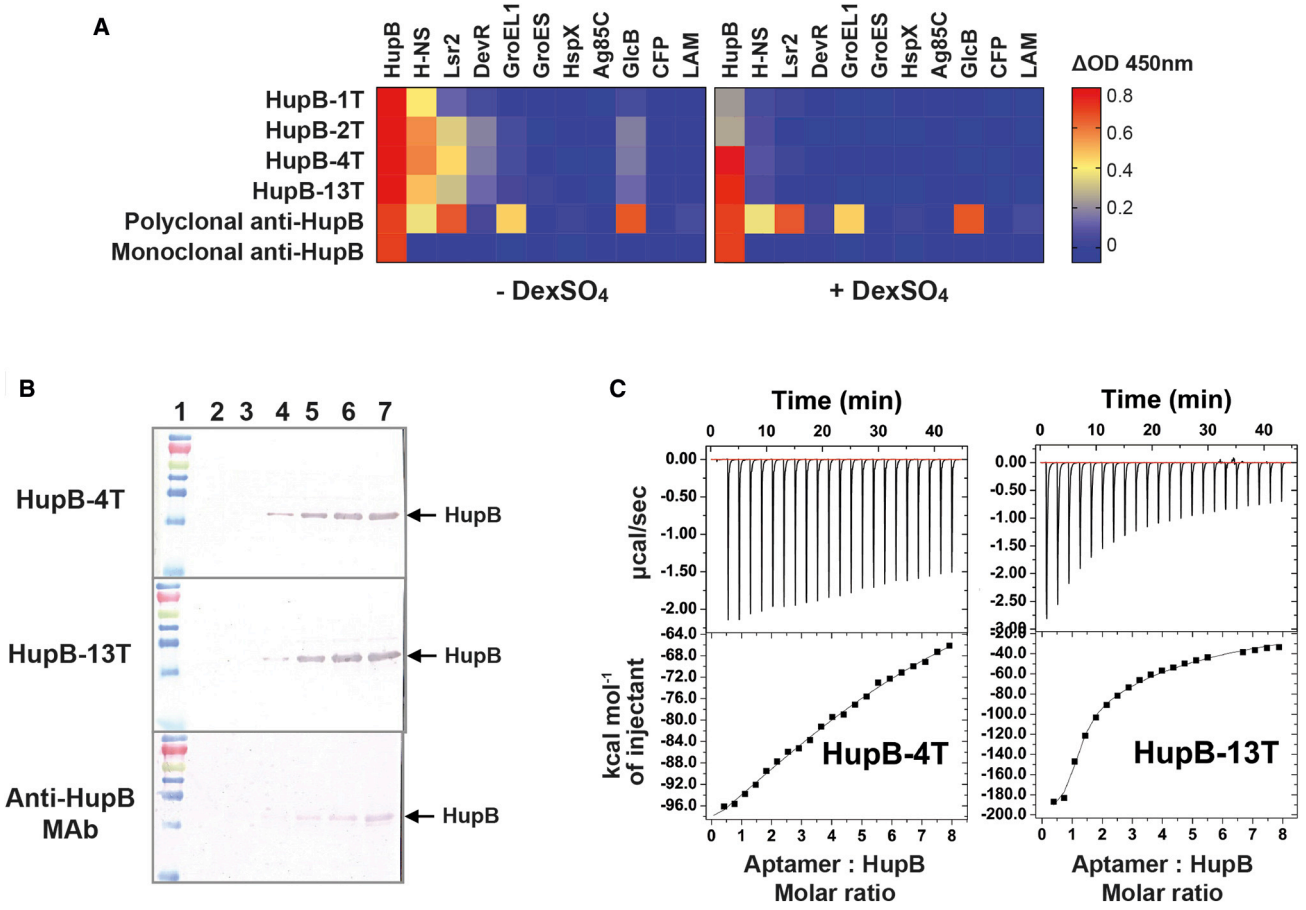

Figure 3. Assessment of Aptamer Selectivity and Affinity

(A) Heatmap representation of ΔOD 450nm values obtained from ALISA using generated aptamers and ELISA carried out using anti-HupB antibodies against various *Mtb* antigens in the absence (–) and presence (+) of 500 nM $DexSO_4$. (B) Western blot analysis of *Mtb* H37Rv whole-cell lysates for detection of endogenous HupB protein (~30 kDa) using HupB-4T, HupB-13T aptamers, or anti-HupB mAb. Lane 1, molecular weight marker; lanes 2 to 7, 1 µg, 2.5 µg, 5 µg, 10 µg, 15 µg, 20 µg proteins of *Mtb* H37Rv whole-cell lysates. (C) Two-site binding of HupB-4T and HupB-13T aptamers to HupB using ITC. Shown are the titrations of HupB into a solution of the aptamer (HupB-4T or HupB-13T). Top, titration data showing the heat resulting from each injection of HupB into an aptamer solution; bottom, integrated heats after correcting for the heat of dilution. Binding experiments were performed at room temperature in selection buffer. See also Table S3 and Figure S3.

counterparts (Figure 2C; *p < 0.05, ***p < 0.005) in agreement with previous reports.[18–20] Accordingly, the truncated (T) aptamers, namely HupB-1T, HupB-2T, HupB-4T and HupB-13T, were used for further studies.

Assessment of Aptamer Selectivity for HupB

The polyanionic compound $DexSO_4$ was used to mask non-specific charge-based interactions of ssDNA aptamers, which are naturally polyanionic in nature,[21,22] with non-target molecules having a positive charge. To assess the specificity of the four selected HupB aptamers, ALISA was carried out with a panel of *Mtb* antigens in the presence and absence of 500 nM $DexSO_4$ and compared to that of previously in-house generated polyclonal and monoclonal anti-HupB antibodies by ELISA. As HupB has a high positive charge (pI 12.48), the aptamers were evaluated against DevR and other DNA-binding proteins having positive charge (H-NS, Lsr2), chaperone proteins (GroEL1, GroES, HspX), cell wall component (Lipoarabinomanan), surface-expressed (GlcB), secretory (Ag85C), and culture filtrate proteins. While all four aptamers bound to HupB, the addition of $DexSO_4$ eliminated non-specific binding of HupB-4T and HupB-13T aptamers to all other *Mtb* proteins, including DNA-binding proteins, without altering their binding to HupB protein (Figure 3A). Importantly, $DexSO_4$, did not alter the binding property of HupB-4T and HupB-13T to HupB, indicating that their interaction with HupB is highly specific and possibly mediated by hydrogen bonding and electrostatic interaction.[23] ITC, described below, confirmed this property. These findings are in concordance with previous reports, where high-affinity slow-off rate modified aptamers (SOMAmers) were generated by masking the non-specific interactions using $DexSO_4$.[21] Notably, the addition of $DexSO_4$ abrogated the binding of HupB-1T and HupB-2T aptamers to all proteins, including HupB, suggesting that their interactions

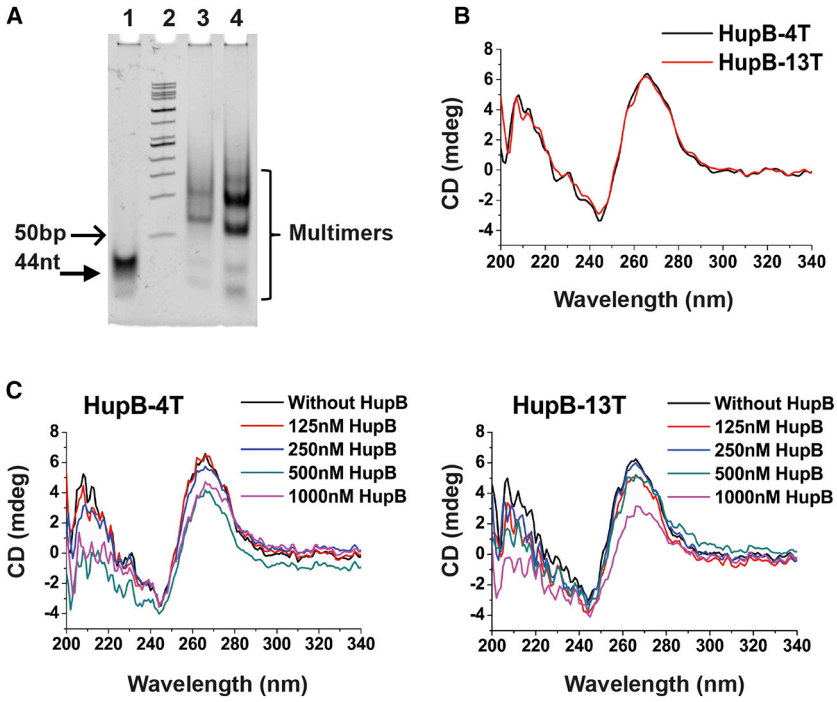

Figure 4. Characterization of HupB-4T and HupB-13T Aptamer Structures

(A) Native PAGE analysis of HupB-4T (lane 3) and HupB-13T (lane 4) aptamers demonstrated the presence of multimers unlike the non-G quadruplex-forming control oligo 1 (lane 1) of the same length. Lane 2, 50 bp DNA ladder. See also Table S4. (B) Circular dichroism spectra of HupB-4T and HupB-13T aptamers reveal the presence of a positive peak near ~260 nm and negative peak near ~240 nm, a typical signature of parallel G-quadruplex structures. (C) CD spectra showing a concentration-dependent target-induced structural change in aptamers in the presence of HupB protein.

were non-specific (Figure 3A). Importantly, HupB-4T and HupB-13T aptamers exhibited high selectivity for HupB that matched that of the monoclonal antibody and was superior to the polyclonal antibody, which exhibited non-specific binding to H-NS, Lsr2, GroEL1, and GlcB proteins. The specificity of HupB-4T and HupB-13T aptamers was further established by specific detection of HupB protein in whole-cell lysates of *Mtb* H37Rv (Figure 3B). Both the aptamers also exhibited superior performance in terms of limit of detection compared to anti-HupB monoclonal antibody (mAb) by western blot (Figure 3B), which is likely due to the use of highly sensitive streptavidin-biotin chemistry with aptamers. Based on these findings, HupB-4T and HupB-13T aptamers were selected for further studies.

HupB-4T and HupB-13T Aptamers Display High-Affinity Binding to HupB

To understand the thermodynamic profile and nature of interactions among HupB-4T, HupB-13T aptamers, and HupB target protein, an ITC analysis was performed (Figure 3C). The ITC data was fitted in a two-site binding model[23,24] that suggested a binding stoichiometry of 2:1 between aptamer molecule and HupB (2 aptamer : 1 HupB protein molecule). ITC data analysis revealed that among the two independent binding sites in HupB (arbitrarily denoted as site 1 and site 2 for each aptamer), the aptamers exhibited higher affinity for one site (assigned as site 1) over the other (assigned as site 2) (Table S3).

For HupB-4T aptamer, ~13 fold higher affinity was observed at site 1 versus site 2, with an estimated K_D of 1.72 ± 0.00002 μM, enthalpy change ΔH of −135 ± 0.0096 kcal/mol, and entropy change ΔS of −0.426 kcal/mol/K. For HupB-13T aptamer, ~122 fold higher affinity was observed at site 1, with estimated K_D of 0.17 ± 0.00000005 μM, enthalpy change ΔH of −207.4 ± 0.0058 kcal/mol, and entropy change ΔS of −0.665 kcal/mol/K. Comparing the K_D values of aptamers at high-affinity sites, HupB-13T aptamer exhibited ~10-fold higher affinity compared to HupB-4T aptamer for HupB. The negative value of net enthalpy change (ΔH) demonstrated the thermodynamically favorable interaction between aptamer and proteins.[25] Further, through ALISA-based competition assay using 5′-biotinylated-HupB-4T (hot probe) and unlabeled HupB-13T aptamers (cold competitor) and vice versa, it was deduced that the binding sites of the two aptamers on HupB were distinct (Figure S3). These findings suggest that aptamer-HupB interactions occurred spontaneously for both aptamers at both the sites, irrespective of their affinity.[23]

Characterization of HupB-4T and HupB-13T Aptamer Structures

The ability of ssDNA aptamers to bind their target molecules is dependent on their 2D and 3D structures. Considering that HupB-4T and HupB-13T aptamers were derived from 50% G- and 60% G+T-biased RDLs and that they have high G and G+T content in their sequences, we assessed the possibility of guanine-quadruplex (G-quadruplex) formation. G-quadruplex structures are often considered to be quite favorable when present in therapeutic aptamers, as they impart high stability, are non-immunogenic, have high cellular uptake, and have enhanced resistance to serum nucleases. We utilized the G4 Predictor tool, G4IPDB[26] (http://bsbe.iiti.ac.in/bsbe/ipdb/pattern2.php), and the prevalent QGRS Mapper[27] tool (http://bioinformatics.ramapo.edu/QGRS/index.php) to predict the number and distribution of quadruplex-forming G-rich sequences (QGRS) with high accuracy.[27,28] Both HupB-4T and HupB-13T aptamers evinced high G scores (range 21–34) that was comparable or even exceeded the QGRS Mapper predicted G scores of established G-quadruplex-forming aptamers such as Thrombin[29] and anti-VEGF[30] (Table S4). Analysis of these aptamers on non-denaturing PAGE provided experimental support, as both HupB-4T and HupB-13T aptamers migrated as multiple bands of higher molecular weight, unlike the control oligo 1 (Figure 4A), confirming formation of intra- (monomer) and inter-molecular structures (di- or tetramers) typically present in G-quadruplex-forming aptamers.[31]

These observations are in accordance with a recent report by Xing et al.[32] who deduced quadruplex structures of their G-rich Kanamycin aptamers through native PAGE analysis.

HupB-4T and HupB-13T Aptamers Undergo Target-Induced Structural Changes

Aptamers are known to undergo target-induced structural changes that can be monitored through CD spectroscopy.[18] Moreover, this technique can reveal secondary structure (B-DNA, stem-loop, etc.) including G-quadruplex formation in aptamers. Parallel G-quadruplex structures typically display a negative peak at 240 to 245 nm and a positive peak at 260 to 265 nm, while antiparallel G-quadruplex structures display a negative peak at 260 to 265 nm and a positive peak at 290 to 295 nm.[33–35] CD analysis of HupB-4T and HupB-13T aptamers revealed a negative peak approximately at 240 nm and a positive peak around 260 nm in the spectrum (Figure 4B), confirming the presence of parallel G-quadruplex structures[18,35] in both these aptamers. In the presence of increasing amounts of HupB protein (125 to 1,000 nM), a concentration-dependent change in the molar ellipticity of CD spectra was observed (Figure 4C), suggesting some target-dependent structural change in aptamer as a function of aptamer-protein interactions.[18,36,37]

HupB-4T Aptamer Inhibits DNA-Binding Function of HupB

The primary function of HupB protein in mycobacteria is to modulate chromatin structure and protect the genome from various stresses, such as oxidative damage, nucleases, etc.[4,5,38] The dsDNA-binding activity in HupB was originally attributed to its NTD (Figure S4A), as the CTD was completely devoid of DNA-binding function. However, studies with truncated forms of the protein, together with *in vivo* data, have confirmed that CTD of HupB has an important role in modulating HupB-DNA binding and nucleoid organization processes *in vivo*.[4,5] Here, we show that both HupB-4T and HupB-13T aptamers evinced significantly higher binding to full-length HupB than to the isolated NTD[39] of HupB (Figure S4B; ****$p < 0.0001$), suggesting that these aptamers may preferably interact with the CTD. To assess the effect of aptamer binding on the DNA-binding function of HupB, a 5′-biotinylated *narK2* gene promoter DNA from *Mtb* was generated that naturally possessed a high-affinity HupB-box-like element. Although, mycobacterial HupB protein shows strong interaction with various forms of DNA (linear, repair, replication intermediates, etc.) in a sequence-independent manner,[5,40] it specifically displays superior binding affinity to an ~10-bp DNA motif designated as "HupB-box."[41] We observed significantly reduced interaction between HupB and *narK2* promoter DNA (5′-biotinylated), in presence of increasing amounts of unlabeled HupB-4T and HupB-13T aptamers (Figure 5A). This observation appeared at first to be somewhat counterintuitive, considering that the aptamer-binding site likely mapped in the CTD of HupB, whereas NTD of HupB was assigned the dsDNA-binding function.[5,40] However, in agreement with the reported importance of HupB CTD,[4,5,40] the observed inhibition in dsDNA binding may be explained by disruption of the DNA-binding domain in NTD owing to aptamer-HupB molecular interactions.

Aptamers Bind to HupB on the Bacterial Cell Surface and Inhibit *Mtb* H37Rv Invasion of Host Macrophages

Besides associating with the mycobacterial nucleoid, HupB protein is also reported to be expressed on the mycobacterial surface and function as a putative adhesin.[11] We confirmed the localization of HupB on the cell surface and in the cell wall fraction of *Mtb* H37Rv by immunoelectron microscopy (Figure 5B) and western blot analysis (Figure 5C), respectively. Further, the binding of 5′-FAM-labeled HupB-4T and HupB-13T aptamers to cell-surface-associated HupB of *Mtb* H37Rv was established by flow cytometry, a significant shift in the median fluorescent intensity (MFI) was observed along the fluorescein isothiocyanate (FITC)-A channel relative to unstained or control oligo (5′-FAM Poly-T)-stained bacilli (Figure 5D).

After establishing the cell-surface localization of HupB and binding of aptamers to surface-expressed HupB, the ability of HupB-targeting aptamers to inhibit *Mtb* H37Rv entry into THP-1 cells was assessed next. The stability of HupB-4T and HupB-13T aptamers in serum (which is usually rich in nucleases) was determined before assessing them in an infection model. Normally, G-quadruplex aptamers are reported to naturally resist serum nucleases,[18] which would be an advantageous feature of HupB-4T and HupB-13T aptamers that likely form parallel G-quadruplex structures (Table S4; Figure 4A). Following incubation in fetal bovine serum (FBS) for 3 hr at 37°C, we did not observe any change in the integrity of aptamer bands, monitored by native PAGE (Figure S5) and densitometry analysis (Figure 5E), indicating stability of aptamers in FBS during this experiment.

Next, THP-1 cells were infected with *Mtb* H37Rv that were either not treated or pre-treated with HupB-4T or HupB-13T or control or scrambled aptamers (Table S1) for 2 hr. After eliminating the extracellular *Mtb* by washing and amikacin treatment post-infection, internalized *Mtb* (a measure of infectivity) were enumerated by colony-forming unit (CFU) plating. Compared to untreated *Mtb* (control, 100%), HupB-4T and HupB-13T treated bacteria yielded reduced intracellular CFU: ~57.8% and ~45.5%, respectively ($p < 0.0001$; Figure 5F). Importantly, the addition of scrambled or control oligonucleotides did not significantly alter *Mtb* entry into cells (Figure 5F). No loss in the viability of THP-1 cells was observed on exposure to aptamers, as assessed by trypan blue dye exclusion method (data not shown). Taking together the surface localization of HupB and the ability of HupB-4T and HupB-13T aptamers to bind to surface-associated HupB, the reduced recovery of intracellular *Mtb* is attributed to HupB aptamer-mediated inhibition of bacterial entry into host cells, thereby establishing a functional role of HupB in infection and the utility of aptamer reagents to block *Mtb* infection.

DISCUSSION

The inability to use the structure-based inhibitor design approach because of the intrinsically disordered nature of CTD of HupB was overcome in the present study through the use of a SELEX strategy that did not require prior knowledge of the structure of full-length

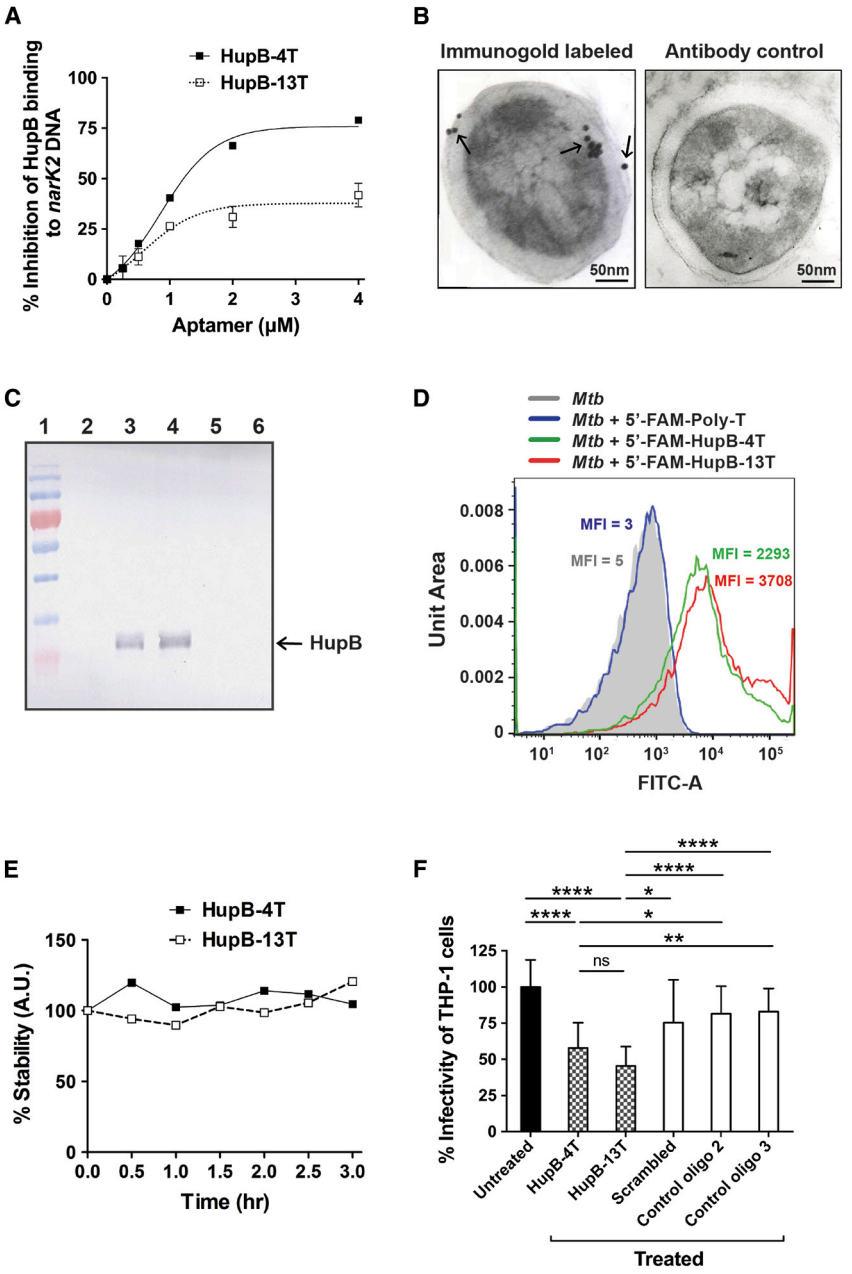

Figure 5. Aptamers HupB-4T and HupB-13T Inhibit Critical Functions of HupB Protein

(A) HupB protein binding to 5′-biotinylated *narK2* promoter dsDNA in the absence and presence of varying concentrations of HupB-4T and HupB-13T aptamers was assessed by ALISA. Data points represent mean ± SD. See also Figure S4. (B) Electron micrographs depicting cell-wall localization of HupB protein in ultra-thin (50 nm) sections of *Mtb*, treated with anti-HupB murine sera, followed by anti-mouse IgG and Protein A-gold conjugate. Scale, 50 nm for immunogold-labeled and antibody control; arrow indicates 15 nm gold particles localized along the exterior and cytosolic side of the cell wall. (C) Immunoblot demonstrating presence of HupB protein in 15 μg *Mtb* H37Rv cell wall fraction and whole-cell lysate using anti-HupB mAb. Lanes 1 to 6, protein molecular weight marker, culture filtrate proteins, whole-cell lysate, cell wall fraction, cell membrane fraction, and cytosol fraction, respectively. (D) Unit-area-normalized histogram overlays depicting significant increase in the median fluorescent intensity (MFI) along the FITC-A channel of gated *Mtb* H37Rv, following incubation with 5′-FAM-labeled HupB-4T (green), or HupB-13T (red) aptamers, compared to 5′-FAM Poly-T (blue) or unstained (gray) control. (E) Stability of HupB-4T and HupB-13T aptamers in arbitrary units (AU) at 37°C in the presence of fetal bovine serum for up to 3 hr assessed by native PAGE and densitometry analysis. Data points represent mean ± SD. See also Figure S5. (F) Percentage infectivity estimated from intracellular CFU count obtained from THP-1 cells infected with *Mtb* H37Rv (10:1 MOI) 2 hr post-infection, following pretreatment with HupB-4T and HupB-13T aptamers and control oligonucleotides (scrambled, control oligos 2 and 3) relative to untreated (100%). *p < 0.05, **p < 0.01, ****p < 0.0001; ns, non-significant. Bars represent mean ± SD.

HupB protein to identify G-quadruplex-forming DNA aptamers against it. For the first time, to the best of our knowledge, we herein report that optimized aptamers against HupB of *Mtb* demonstrate the ability to block two functions of HupB, namely its DNA-binding function and bacterial cell entry into macrophages. The essentiality of *Mtb* HupB is ascribed to its ability to (1) protect mycobacterial DNA from reactive oxygen species (Fenton's reaction) and DNase I digestion,[4–6] as well as (2) maintain iron homeostasis.[8,42] Although mycobacterial *hupB* knockout strains remain viable, differences between wild-type and knockout strains have been observed, e.g., *Mycobacterium smegmatis* knockout strain shows enhanced sensitivity to cold shock, to UV treatment, and to exposure to Isoniazid,[10] whereas an *Mtb* knockout strain fails to gain entry and proliferate within host cells.[8] In several mycobacterial species, such as *M. leprae*,[43] *M. smegmatis*,[44] and *M. bovis* BCG,[45] the corresponding HupB orthologs have been proven to function as adhesin molecules. Therefore, inhibiting HupB-DNA-binding activity along with adhesion and/or invasion of *Mtb* into host cells establishes a crucial checkpoint to block bacterial survival under stress conditions and prevent *Mtb* infection and dissemination. These activities of HupB were significantly inhibited by the aptamers identified in the present study.

The DNA-binding motifs within HupB were first characterized in its stable NTD, as the CTD was noted to be devoid of them.[5,40] Utilizing the structural information of NTD, diarylethene derivatives were recently reported that inhibited HupB binding to DNA and blocked the growth of axenic *Mtb* cultures *in vitro*.[12,13] However, only recently has the importance of HupB CTD in modulating NTD driven DNA processes *in vitro* and *in vivo* been reported.[4,5,40] Moreover,

M. smegmatis strains expressing $HupB_{\Delta CTD}$ as well as *M. smegmatis ΔhupB*[10] exhibited higher sensitivity to Isoniazid, compared to wild-type bacteria.[4] Further, using truncated forms of *M. leprae* HupB protein, the laminin-binding adhesive domain in HupB was localized in its CTD.[13] Therefore, it stands to reason that inhibitors targeting the multifunctional full-length HupB protein are likely to exhibit higher potency.

The most active aptamers, HupB-4T and HupB-13T, each demonstrated 2:1 binding stoichiometry with HupB, with variable affinity at each independent site. Moreover, negative value of Gibb's free-energy change ($\Delta G < 0$) in ITC assay indicated a spontaneous binding of aptamers to HupB. Although aptamer-mediated multisite binding is less frequent, there are reports in the literature that testify to its occurrence, e.g., cocaine-binding aptamer,[46] ATP-binding aptamer,[47,48] and neomycin B-binding aptamer.[49] In our study, the K_D at high-affinity sites for both the aptamers was in the low micromolar range, thereby explaining the superior binding properties of aptamers in comparison to mono- and polyclonal antibodies. These findings are in agreement with the superior binding property of aptamers compared to polyclonal antibody reported for the detection of tularemia total bacterial antigen.[50] High-affinity and stable interactions displayed by both HupB-4T and HupB-13T aptamers is also conceivably sustained by their parallel G-quadruplex structures (Figure 4).

As both HupB-4T and HupB-13T aptamers evinced ≥ 4 fold higher binding to the full-length HupB protein than the isolated NTD (Figure S4B), it is inferred that either the aptamers preferentially bound the CTD of HupB or specifically required both the domains for efficient binding. In either case, it must be noted that the HupB binding sites of HupB-4T and HupB-13T aptamers were confirmed to be distinct and non-overlapping. In spite of HupB-13T aptamer having a ~10-fold higher affinity for HupB (Table S3), it inhibited HupB DNA-binding activity by only ~25% compared to HupB-4T aptamer that inhibited HupB binding to DNA by ~75% (Figure 5A). These observations collectively suggest that HupB-4T interacts with critical residues in HupB CTD that modulate the DNA-binding function of HupB NTD. The maximum inhibition of HupB-DNA interaction achieved through HupB-4T aptamer saturated at ~75%. The residual DNA-binding activity (~25%) can be explained by the intrinsic DNA-binding property of HupB NTD.[40]

As *Mtb ΔhupB* mutant bacteria fail to enter and survive inside host cells,[8] a second logical check point for intercepting *Mtb* infection and dissemination by inhibiting *Mtb* entry into host cells by blocking HupB. HupB expression on the mycobacterial surface (Figures 5B and 5C) and the binding of HupB-4T and HupB-13T aptamers to *Mtb* (Figure 5D) was seen to significantly antagonize *Mtb* invasion into THP-1 cells. Thus, the aptamers described here target an important virulence property of *Mtb*; that is, its ability to gain entry into mammalian cells. Over the years, several mycobacterial surface ligands besides HupB have been identified that facilitate bacterial entry by engaging a wide array of host cell adhesion molecules and immune receptors, e.g., ManLAM,[51] LprG,[52] PIMs,[53] Mce1,[54] PE_PGRS33,[55] and adhesins including HBHA,[56] Apa,[57] GlcB,[58] and 19-kDa antigen.[59] It is therefore crucial to note that, in this study, by blocking of only a single protein, HupB, a high degree of inhibition of *Mtb* infection (~40%–55%) was achieved. In comparison, although a similar degree of aptamer-mediated inhibition of *Mtb* adhesion and/or invasion in host cells was previously reported by Chen et al.,[60] the identity of their target molecule is unknown, as their aptamers were evolved against whole *Mtb* cells. Due to a lack of distinct target site information in their study and the known antigenic variation in *Mtb* surface proteins, the utility of their aptamer may vary among different strains. In contrast, HupB is an essential protein, and intercepting the DNA-binding function and adhesin function of HupB with aptamers has significant therapeutic potential.

In conclusion, *Mtb* HupB has been suggested to be a potent drug target;[3,12,13] however, the lack of structural knowledge of the full-length protein has impeded the development of potent inhibitors. In the current study, we have overcome this limitation by exploiting SELEX technology, which does not require structural information of the target to develop target specific inhibitors. We have identified and characterized aptamers that show high stability, affinity, and selectivity for *Mtb* HupB protein. The best performing aptamer candidates, HupB-4T and HupB-13T, evinced robust inhibition of key functions of HupB, namely its DNA-binding function and mycobacterial invasion within host cells. Taken together with their serum stability, non-toxic properties and the possibility to optimize them further for improved potency, these HupB aptamers have significant potential to be developed as potent biocompatible inhibitors of *Mtb* survival.

MATERIALS AND METHODS

Reagents and Chemicals

All routine reagents were procured from Sigma Aldrich, USA, and Thermo Fisher Scientific, USA, unless otherwise mentioned. Primers, DNA library, and other oligonucleotides used in the study were procured from Integrated DNA Technologies, USA. Nitrocellulose (NCM) and polyvinylidene fluoride (PVDF) membrane was obtained from mdi, Ambala, India. *Mtb* H37Rv was cultured in Difco Middlebrook 7H9 broth (BD Biosciences, USA) supplemented with 10% Albumin-Dextrose-NaCl (ADN). *Mtb* H37Rv cell fractions and proteins were obtained from BEI Resources, NIAID, NIH, USA (detailed in Supplemental Materials and Methods). Recombinant His_6-tagged HupB, NTD-HupB, DevR, GlcB, Lsr2, and H-NS proteins of *Mtb* H37Rv were expressed in *E. coli* and purified by Ni^+-NTA affinity chromatography by standard procedures. Anti-HupB monoclonal and polyclonal antibody (V. Gupta, P.K., and H.K.P., unpublished data) was generated in-house.

SELEX

An equimolar mixture of two G-quadruplex-biased (50% G and 60% G+T) and one unbiased (completely random) ~80nt length ss random DNA libraries (RDLs) were used (5′-GTCTTGACTAGT TACGCC-*N3-**X41-TCATTCAGTTGGCGCCTC-3′; *, **; Table S1), having a central *N = 3nt sequence tag and **X = 41nt random

region (biased or unbiased) flanked by 5′ and 3′ primer binding sites (18 nt each), to enable amplification by PCR using DRF (5′-GTCT TGACTAGTTACGCC-3′) and DRR primers (5′-GAGGCGCCAAC TGAATGA-3′). Using a cocktail of these RDLs, subtractive SELEX methodology described by Cao et al.[61] was followed for aptamer selection, with modifications as detailed in the Supplemental Materials and Methods.

ALISA

In brief, 500ng/well recombinant HupB protein was coated overnight using standard 100 mM carbonate-bicarbonate buffer, pH 9.6 at 4°C. After washing with selection buffer (SB; 10 mM Tris, pH 7.5, 10 mM $MgCl_2$, 50 mM KCl, 25 mM NaCl) and blocking with 5% skimmed milk for 90 min at room temperature (RT), the optimized amount of prepared or commercially obtained 5′-biotin labeled ssDNA was added to wells for 60 min at RT. After washing with SB supplemented with 0.5% Tween 20 (v/v), streptavidin-horseradish peroxidase (HRP) (Sigma) was added at 1:1,500 dilution and incubated for 1 hr at RT. ALISA was developed using 100 µL OptEIA TMB substrate, (3,3′,5,5′-tetramethylbenzidine; BD Biosciences, USA), the reaction quenched using 5% H_2SO_4 and optical density (OD) measured at 450 nm. ΔOD 450 nm estimated by subtracting OD 450 nm of appropriate negative controls (aptamer control, antigen control, etc.) was plotted.

ITC

All ITC experiments were performed using a MicroCal ITC200 instrument (GE Healthcare, USA) at 25°C and corrected for heat of dilution of the titrant. All samples were degassed prior to each experiment. All titrations were performed with the aptamers in the syringe and the protein in the cell. Binding experiments consisted of 22 successive injections spaced every 180 s, where the first injection was of 0.4 µL that accounted for diffusion from the syringe into the cell during equilibration. For each ITC experiment, 50 µM of aptamer and 2.5 µM of HupB protein was dissolved in SB and data was generated. Based on the best curve fit, the data was fitted into two independent sites binding model[62] using manufacturer-provided data-fitting package within Origin 7, SR4 software (OriginLab). Dissociation constant (K_D) was calculated using the formula $K_D = 1/K_A$, where K_A is association constant of the tested aptamer candidate. Free energy change (ΔG) was calculated using the Gibbs free-energy equation; $\Delta G = \Delta H - T\Delta S$; where ΔH and ΔS are changes in enthalpy and entropy, respectively.

CD Study

The average of three scans of CD spectra (mdeg; ChiraScan, Applied Photophysics) between 200 and 340 nm at a step size of 1 nm was determined for HupB-4Tand HupB-13T aptamers (5 µM). In addition, the CD spectra of these aptamers (5 µM) were determined in the presence of a range of HupB protein (125, 250, 500, 1,000 nM) to assess target-dependent changes in aptamer structure. The data was fitted using Origin 7, SR4 software (OriginLab Corporation).

Inhibition of *Mtb* H37Rv Invasion in THP-1 Cells

The protocol described by Chen et al.[60] was used with slight modifications to assess aptamer-mediated inhibition of *Mtb* H37Rv infectivity. In brief, 5×10^6 *Mtb* H37Rv were either pre-treated or not treated with 8 µg aptamers (4 µM; HupB-4T or HupB-13T) or control oligonucleotides (scrambled, control oligo 2, or control oligo 3; Table S1) for 1 hr at 37°C. Thereafter, 0.5×10^6 THP-1 cells, cultured in 10% FBS supplemented RPMI 1640 media, were infected with untreated or aptamer pre-treated 5×10^6 *Mtb* H37Rv (10:1 MOI) for 2 hr at 37°C. Extracellular *Mtb* were eliminated by washing and treatment with 200 µg/mL Amikacin for 2 hr. After thorough washing, the cells were lysed using 0.025% SDS and the lysates plated on 7H11 agar at various dilutions. After 5 weeks, intracellular *Mtb* H37Rv CFU/mL were enumerated and compared with respect to untreated *Mtb* H37Rv taken as control (100%).

Statistical Analysis

All experimental data are represented as mean ± SD that was determined using the unpaired two-tailed Student's t test in GraphPad Prism v7.0 software. p values ≤ 0.05 were considered statistically significant and represented as $^*p \leq 0.05$; $^{**}p \leq 0.01$; $^{***}p \leq 0.005$; $^{****}p \leq 0.001$.

Additional details regarding methods are presented in the Supplemental Information.

SUPPLEMENTAL INFORMATION

Supplemental Information includes Supplemental Materials and Methods, five figures, and four tables and can be found with this article online at https://doi.org/10.1016/j.omtn.2018.08.011.

AUTHOR CONTRIBUTIONS

J.S.T., H.K.P., and T.K.S. conceived the idea. J.S.T., H.K.P., A.K., and T.K.S. designed and supervised the experiments. P.K., S.K.M., and S.K. performed experiments and collected and analyzed data. P.K., J.S.T., H.K.P., T.K.S., S.K.M., and A.K. wrote the manuscript and contributed to data analysis. All authors reviewed the manuscript.

CONFLICTS OF INTEREST

The aptamer sequences reported in this study are proprietary reagents and are deposited in the Indian Patent Office as part of Indian Patent application no. 201711001246.

ACKNOWLEDGMENTS

The Department of Biotechnology, Government of India, is acknowledged for supporting this work through the National Biodesign Alliance project (BT/PR14638/MED/12/483/2010) to J.S.T., the Innovation Award to T.K.S., and a Senior Research Fellowship to P.K. T.K.S. thanks the Translational Health Science & Technology Institute, Faridabad for providing core grant support. T.K.S. also thanks the Department of Biotechnology, Government of India for the DBT-Innovative Young Biotechnologist Award (BT/010/IYBA/2016/10). H.K.P. thanks the Indian Council of Medical Research, Government of India for the award of an Emeritus Medical Scientist

position. S.K.M. acknowledges the University Grants Commission, Government of India for the Senior Research Fellowship (22/06/2014 (i) EU-V). *Mtb* H37Rv was a kind gift from Dr. Richard F. Silver, Case Western Reserve University, Cleveland, OH, USA. The THP-1 cell line was a kind gift from Dr. Nasreen Z. Ehtesham, National Institute of Pathology, New Delhi, India. BEI Resources, NIAID, and NIH are acknowledged for providing cell fractions and various proteins of *Mtb* and strain H37Rv.

REFERENCES

1. World Health Organization (2017). Global Tuberculosis Report. http://www.who.int/tb/publications/global_report/en/.
2. Griffin, J.E., Gawronski, J.D., Dejesus, M.A., Ioerger, T.R., Akerley, B.J., and Sassetti, C.M. (2011). High-resolution phenotypic profiling defines genes essential for mycobacterial growth and cholesterol catabolism. PLoS Pathog. *7*, e1002251.
3. Sassetti, C.M., Boyd, D.H., and Rubin, E.J. (2003). Genes required for mycobacterial growth defined by high density mutagenesis. Mol. Microbiol. *48*, 77–84.
4. Hołówka, J., Trojanowski, D., Ginda, K., Wojtaś, B., Gielniewski, B., Jakimowicz, D., and Zakrzewska-Czerwińska, J. (2017). HupB Is a Bacterial Nucleoid-Associated Protein with an Indispensable Eukaryotic-Like Tail. MBio *8*, e01272–17.
5. Kumar, S., Sardesai, A.A., Basu, D., Muniyappa, K., and Hasnain, S.E. (2010). DNA clasping by mycobacterial HU: the C-terminal region of HupB mediates increased specificity of DNA binding. PLoS ONE *5*, e12551.
6. Prabhakar, S., Annapurna, P.S., Jain, N.K., Dey, A.B., Tyagi, J.S., and Prasad, H.K. (1998). Identification of an immunogenic histone-like protein (HLPMt) of Mycobacterium tuberculosis. Tuber. Lung Dis. *79*, 43–53.
7. Pethe, K., Bifani, P., Drobecq, H., Sergheraert, C., Debrie, A.S., Locht, C., and Menozzi, F.D. (2002). Mycobacterial heparin-binding hemagglutinin and laminin-binding protein share antigenic methyllysines that confer resistance to proteolysis. Proc. Natl. Acad. Sci. USA *99*, 10759–10764.
8. Pandey, S.D., Choudhury, M., Yousuf, S., Wheeler, P.R., Gordon, S.V., Ranjan, A., and Sritharan, M. (2014). Iron-regulated protein HupB of Mycobacterium tuberculosis positively regulates siderophore biosynthesis and is essential for growth in macrophages. J. Bacteriol. *196*, 1853–1865.
9. Niki, M., Niki, M., Tateishi, Y., Ozeki, Y., Kirikae, T., Lewin, A., Inoue, Y., Matsumoto, M., Dahl, J.L., Ogura, H., et al. (2012). A novel mechanism of growth phase-dependent tolerance to isoniazid in mycobacteria. J. Biol. Chem. *287*, 27743–27752.
10. Whiteford, D.C., Klingelhoets, J.J., Bambenek, M.H., and Dahl, J.L. (2011). Deletion of the histone-like protein (Hlp) from Mycobacterium smegmatis results in increased sensitivity to UV exposure, freezing and isoniazid. Microbiology *157*, 327–335.
11. Bhowmick, T., Ghosh, S., Dixit, K., Ganesan, V., Ramagopal, U.A., Dey, D., Sarma, S.P., Ramakumar, S., and Nagaraja, V. (2014). Targeting Mycobacterium tuberculosis nucleoid-associated protein HU with structure-based inhibitors. Nat. Commun. *5*, 4124.
12. Suarez, M.A., Valencia, J., Cadena, C.C., Maiti, R., Datta, C., Puerto, G., Isaza, J.H., San Juan, H., Nagaraja, V., and Guzman, J.D. (2017). Diarylethenes Display In Vitro Anti-TB Activity and Are Efficient Hits Targeting the Mycobacterium tuberculosis HU Protein. Molecules *22*, E1245.
13. Soares de Lima, C., Zulianello, L., Marques, M.A. de M., Kim, H., Portugal, M.I., Antunes, S.L., Menozzi, F.D., Ottenhoff, T.H., Brennan, P.J., and Pessolani, M.C. (2005). Mapping the laminin-binding and adhesive domain of the cell surface-associated Hlp/LBP protein from Mycobacterium leprae. Microbes Infect. *7*, 1097–1109.
14. Baig, I.A., Moon, J.Y., Lee, S.C., Ryoo, S.W., and Yoon, M.Y. (2015). Development of ssDNA aptamers as potent inhibitors of Mycobacterium tuberculosis acetohydroxyacid synthase. Biochim. Biophys. Acta *1854* (10 Pt A), 1338–1350.
15. Shum, K.T., Lui, E.L.H., Wong, S.C.K., Yeung, P., Sam, L., Wang, Y., Watt, R.M., and Tanner, J.A. (2011). Aptamer-mediated inhibition of Mycobacterium tuberculosis polyphosphate kinase 2. Biochemistry *50*, 3261–3271.
16. Bruno, J.G. (2016). Automated aptamer development may represent the last and best line of defense against proverbial "Doomsday" pathogens. Aptamers Synth. Antibodies *2*, 13–17.
17. Tabarzad, M., Kazemi, B., Vahidi, H., Aboofazeli, R., Shahhosseini, S., and Nafissi-Varcheh, N. (2014). Challenges to design and develop of DNA aptamers for protein targets. I. Optimization of asymmetric PCR for generation of a single stranded DNA library. Iran. J. Pharm. Res. *13* (*Suppl*), 133–141.
18. Sharma, T.K., Bruno, J.G., and Dhiman, A. (2017). ABCs of DNA aptamer and related assay development. Biotechnol. Adv. *35*, 275–301.
19. Macdonald, J., Houghton, P., Xiang, D., Duan, W., and Shigdar, S. (2016). Truncation and Mutation of a Transferrin Receptor Aptamer Enhances Binding Affinity. Nucleic Acid Ther. *26*, 348–354.
20. Kaur, H., and Yung, L.Y.L. (2012). Probing high affinity sequences of DNA aptamer against VEGF165. PLoS ONE *7*, e31196.
21. Gold, L., Ayers, D., Bertino, J., Bock, C., Bock, A., Brody, E.N., Carter, J., Dalby, A.B., Eaton, B.E., Fitzwater, T., et al. (2010). Aptamer-based multiplexed proteomic technology for biomarker discovery. PLoS ONE *5*, e15004.
22. Kalra, P., Dhiman, A., Cho, W.C., Bruno, J.G., and Sharma, T.K. (2018). Simple Methods and Rational Design for Enhancing Aptamer Sensitivity and Specificity. Front. Mol. Biosci. *5*, 41.
23. Freyer, M.W., and Lewis, E.A. (2008). Isothermal titration calorimetry: experimental design, data analysis, and probing macromolecule/ligand binding and kinetic interactions. Methods Cell Biol. *84*, 79–113.
24. Brautigam, C.A. (2015). Fitting two- and three-site binding models to isothermal titration calorimetric data. Methods *76*, 124–136.
25. Du, X., Li, Y., Xia, Y.L., Ai, S.M., Liang, J., Sang, P., Ji, X.L., and Liu, S.Q. (2016). Insights into Protein-Ligand Interactions: Mechanisms, Models, and Methods. Int. J. Mol. Sci. *17*, E144.
26. Mishra, S.K., Tawani, A., Mishra, A., and Kumar, A. (2016). G4IPDB: A database for G-quadruplex structure forming nucleic acid interacting proteins. Sci. Rep. *6*, 38144.
27. Kikin, O., D'Antonio, L., and Bagga, P.S. (2006). QGRS Mapper: a web-based server for predicting G-quadruplexes in nucleotide sequences. Nucleic Acids Res. *34*, W676-82.
28. Viglasky, V., and Hianik, T. (2013). Potential uses of G-quadruplex-forming aptamers. Gen. Physiol. Biophys. *32*, 149–172.
29. Bock, L.C., Griffin, L.C., Latham, J.A., Vermaas, E.H., and Toole, J.J. (1992). Selection of single-stranded DNA molecules that bind and inhibit human thrombin. Nature *355*, 564–566.
30. Nonaka, Y., Sode, K., and Ikebukuro, K. (2010). Screening and improvement of an anti-VEGF DNA aptamer. Molecules *15*, 215–225.
31. Tóthová, P., Krafčíková, P., and Víglaský, V. (2014). Formation of highly ordered multimers in G-quadruplexes. Biochemistry *53*, 7013–7027.
32. Xing, Y.P., Liu, C., Zhou, X.H., and Shi, H.C. (2015). Label-free detection of kanamycin based on a G-quadruplex DNA aptamer-based fluorescent intercalator displacement assay. Sci. Rep. *5*, 8125.
33. Fujita, H., Imaizumi, Y., Kasahara, Y., Kitadume, S., Ozaki, H., Kuwahara, M., and Sugimoto, N. (2013). Structural and affinity analyses of g-quadruplex DNA aptamers for camptothecin derivatives. Pharmaceuticals (Basel) *6*, 1082–1093.
34. Kypr, J., Kejnovská, I., Renciuk, D., and Vorlíčková, M. (2009). Circular dichroism and conformational polymorphism of DNA. Nucleic Acids Res. *37*, 1713–1725.
35. Paramasivan, S., Rujan, I., and Bolton, P.H. (2007). Circular dichroism of quadruplex DNAs: applications to structure, cation effects and ligand binding. Methods *43*, 324–331.
36. Weerathunge, P., Ramanathan, R., Shukla, R., Sharma, T.K., and Bansal, V. (2014). Aptamer-controlled reversible inhibition of gold nanozyme activity for pesticide sensing. Anal. Chem. *86*, 11937–11941.
37. Lin, P.H., Tsai, C.W., Wu, J.W., Ruaan, R.C., and Chen, W.Y. (2012). Molecular dynamics simulation of the induced-fit binding process of DNA aptamer and L-arginamide. Biotechnol. J. *7*, 1367–1375.
38. Gupta, M., Sajid, A., Sharma, K., Ghosh, S., Arora, G., Singh, R., Nagaraja, V., Tandon, V., and Singh, Y. (2014). HupB, a nucleoid-associated protein of

Mycobacterium tuberculosis, is modified by serine/threonine protein kinases in vivo. J. Bacteriol. *196*, 2646–2657.

39. Ghosh, S., Mallick, B., and Nagaraja, V. (2014). Direct regulation of topoisomerase activity by a nucleoid-associated protein. Nucleic Acids Res. *42*, 11156–11165.

40. Sharadamma, N., Khan, K., Kumar, S., Patil, K.N., Hasnain, S.E., and Muniyappa, K. (2011). Synergy between the N-terminal and C-terminal domains of Mycobacterium tuberculosis HupB is essential for high-affinity binding, DNA supercoiling and inhibition of RecA-promoted strand exchange. FEBS J. *278*, 3447–3462.

41. Pandey, S.D., Choudhury, M., and Sritharan, M. (2014). Transcriptional regulation of Mycobacterium tuberculosis hupB gene expression. Microbiology *160*, 1637–1647.

42. Yeruva, V.C., Duggirala, S., Lakshmi, V., Kolarich, D., Altmann, F., and Sritharan, M. (2006). Identification and characterization of a major cell wall-associated iron-regulated envelope protein (Irep-28) in Mycobacterium tuberculosis. Clin. Vaccine Immunol. *13*, 1137–1142.

43. Shimoji, Y., Ng, V., Matsumura, K., Fischetti, V.A., and Rambukkana, A. (1999). A 21-kDa surface protein of Mycobacterium leprae binds peripheral nerve laminin-2 and mediates Schwann cell invasion. Proc. Natl. Acad. Sci. USA *96*, 9857–9862.

44. Pethe, K., Puech, V., Daffé, M., Josenhans, C., Drobecq, H., Locht, C., and Menozzi, F.D. (2001). Mycobacterium smegmatis laminin-binding glycoprotein shares epitopes with Mycobacterium tuberculosis heparin-binding haemagglutinin. Mol. Microbiol. *39*, 89–99.

45. Aoki, K., Matsumoto, S., Hirayama, Y., Wada, T., Ozeki, Y., Niki, M., Domenech, P., Umemori, K., Yamamoto, S., Mineda, A., et al. (2004). Extracellular mycobacterial DNA-binding protein 1 participates in mycobacterium-lung epithelial cell interaction through hyaluronic acid. J. Biol. Chem. *279*, 39798–39806.

46. Neves, M.A.D., Slavkovic, S., Churcher, Z.R., and Johnson, P.E. (2017). Salt-mediated two-site ligand binding by the cocaine-binding aptamer. Nucleic Acids Res. *45*, 1041–1048.

47. Huizenga, D.E., and Szostak, J.W. (1995). A DNA aptamer that binds adenosine and ATP. Biochemistry *34*, 656–665.

48. Lin, C.H., and Patel, D.J. (1997). Structural basis of DNA folding and recognition in an AMP-DNA aptamer complex: distinct architectures but common recognition motifs for DNA and RNA aptamers complexed to AMP. Chem. Biol. *4*, 817–832.

49. Cowan, J.A., Ohyama, T., Wang, D., and Natarajan, K. (2000). Recognition of a cognate RNA aptamer by neomycin B: quantitative evaluation of hydrogen bonding and electrostatic interactions. Nucleic Acids Res. *28*, 2935–2942.

50. Vivekananda, J., and Kiel, J.L. (2006). Anti-Francisella tularensis DNA aptamers detect tularemia antigen from different subspecies by Aptamer-Linked Immobilized Sorbent Assay. Lab. Invest. *86*, 610–618.

51. Strohmeier, G.R., and Fenton, M.J. (1999). Roles of lipoarabinomannan in the pathogenesis of tuberculosis. Microbes Infect. *1*, 709–717.

52. Gaur, R.L., Ren, K., Blumenthal, A., Bhamidi, S., González-Nilo, F.D., Jackson, M., Zare, R.N., Ehrt, S., Ernst, J.D., and Banaei, N. (2014). LprG-mediated surface expression of lipoarabinomannan is essential for virulence of Mycobacterium tuberculosis. PLoS Pathog. *10*, e1004376.

53. Villeneuve, C., Gilleron, M., Maridonneau-Parini, I., Daffé, M., Astarie-Dequeker, C., and Etienne, G. (2005). Mycobacteria use their surface-exposed glycolipids to infect human macrophages through a receptor-dependent process. J. Lipid Res. *46*, 475–483.

54. Chitale, S., Ehrt, S., Kawamura, I., Fujimura, T., Shimono, N., Anand, N., Lu, S., Cohen-Gould, L., and Riley, L.W. (2001). Recombinant Mycobacterium tuberculosis protein associated with mammalian cell entry. Cell. Microbiol. *3*, 247–254.

55. Palucci, I., Camassa, S., Cascioferro, A., Sali, M., Anoosheh, S., Zumbo, A., Minerva, M., Iantomasi, R., De Maio, F., Di Sante, G., et al. (2016). PE_PGRS33 Contributes to Mycobacterium tuberculosis Entry in Macrophages through Interaction with TLR2. PLoS ONE *11*, e0150800.

56. Lebrun, P., Raze, D., Fritzinger, B., Wieruszeski, J.M., Biet, F., Dose, A., Carpentier, M., Schwarzer, D., Allain, F., Lippens, G., and Locht, C. (2012). Differential contribution of the repeats to heparin binding of HBHA, a major adhesin of Mycobacterium tuberculosis. PLoS ONE *7*, e32421.

57. Ragas, A., Roussel, L., Puzo, G., and Rivière, M. (2007). The Mycobacterium tuberculosis cell-surface glycoprotein apa as a potential adhesin to colonize target cells via the innate immune system pulmonary C-type lectin surfactant protein A. J. Biol. Chem. *282*, 5133–5142.

58. Kinhikar, A.G., Vargas, D., Li, H., Mahaffey, S.B., Hinds, L., Belisle, J.T., and Laal, S. (2006). Mycobacterium tuberculosis malate synthase is a laminin-binding adhesin. Mol. Microbiol. *60*, 999–1013.

59. Diaz-Silvestre, H., Espinosa-Cueto, P., Sanchez-Gonzalez, A., Esparza-Ceron, M.A., Pereira-Suarez, A.L., Bernal-Fernandez, G., Espitia, C., and Mancilla, R. (2005). The 19-kDa antigen of Mycobacterium tuberculosis is a major adhesin that binds the mannose receptor of THP-1 monocytic cells and promotes phagocytosis of mycobacteria. Microb. Pathog. *39*, 97–107.

60. Chen, F., Zhang, X., Zhou, J., Liu, S., and Liu, J. (2012). Aptamer inhibits Mycobacterium tuberculosis (H37Rv) invasion of macrophage. Mol. Biol. Rep. *39*, 2157–2162.

61. Cao, X., Li, S., Chen, L., Ding, H., Xu, H., Huang, Y., Li, J., Liu, N., Cao, W., Zhu, Y., et al. (2009). Combining use of a panel of ssDNA aptamers in the detection of Staphylococcus aureus. Nucleic Acids Res. *37*, 4621–4628.

62. Freiburger, L.A., Auclair, K., and Mittermaier, A.K. (2009). Elucidating protein binding mechanisms by variable-c ITC. ChemBioChem *10*, 2871–2873.